Designed formation of double-shelled ni–fe layered-double-hydroxide nanocages for efficient oxygen evolution reaction

Zhang, Jintao; Yu, Le; Chen, Ye; Lu, Xue Feng; Gao, Shuyan; Lou, David Xiong Wen

2020

Zhang, J., Yu, L., Chen, Y., Lu, X. F., Gao, S., & Lou, D. X. W. (2020). Designed formation of double-shelled Ni–Fe layered-double-hydroxide nanocages for efficient oxygen evolution reaction. Advanced Materials, 32(16), 1906432-. doi:10.1002/adma.201906432

https://hdl.handle.net/10356/138574

https://doi.org/10.1002/adma.201906432

Designed Formation of Double-Shelled Ni-Fe Layered Double Hydroxide Nanocages for Efficient Oxygen Evolution Reaction

Jintao Zhang, Le Yu, Ye Chen, Xue Feng Lu, Shuyan Gao, and Xiong Wen (David) Lou**

[*] Dr. Y. Chen, Prof. S. Y. Gao
School of Chemistry and Chemical Engineering, Henan Normal University, Xinxiang, Henan 453007, P.R. China. Email: shuyangao@htu.cn

Dr. J. T. Zhang, Dr. L. Yu, Dr. X. F. Lu, Prof. X. W. Lou
School of Chemical and Biomedical Engineering, Nanyang Technological University, 62 Nanyang Drive, Singapore 637459, Singapore
Email: xwlou@ntu.edu.sg; Webpage: http://www.ntu.edu.sg/home/xwlou/

Abstract:

Delicate design of nanostructures for oxygen-evolution electrocatalysts is an important strategy for accelerating the reaction kinetics of water splitting. In this work, Ni-Fe layered double hydroxide (LDH) nanocages with tunable shells are synthesized via a facile one-pot self-templated method. The number of shells can be precisely controlled by regulating the template etching at the interface. Benefiting from the double-shelled structure with large electroactive surface area and optimized chemical composition, the hierarchical Ni-Fe LDH nanocages exhibit appealing electrocatalytic activity for the oxygen evolution reaction in alkaline electrolyte. Particularly, double-shelled Ni-Fe LDH nanocages could achieve the current density of 20 mA cm^{-2} at a low overpotential of 246 mV with excellent stability.

Keywords: Ni-Fe, layered double hydroxide, double-shelled, nanocages, oxygen evolution reaction

The fast depletion of fossil fuels and the ever-growing concerns over carbon dioxide emission advance the development of sustainable and environmentally friendly fuel sources.[1, 2] Among variable alternatives, hydrogen has been considered as one ideal energy carrier because its combustion product is no more than water.[3-5] Electrochemical water splitting is one of the most promising strategies to create high-purity hydrogen on a large scale in a green and economic way.[6, 7] During this fuel production process, the oxygen evolution reaction (OER) is regarded as the bottleneck due to its sluggish reaction kinetics with non-negligible overpotential (η), even using comparatively high-activity catalysts (such as IrO_2 and RuO_2).[8] Additionally, the high cost and scarcity of such noble metal-based catalysts always limit their large-scale application. In this regard, substantial efforts have been devoted to developing cost-effective and highly active electrocatalysts for replacing the state-of-the-art precious metal-based catalysts.[9]

First-row transition-metal oxides, hydroxides, sulfides, nitrides, and phosphides have attracted significant attention as the next-generation catalysts for OER in view of the earth abundance and high catalytic activity.[4, 10-17] In particular, Ni-Fe layered double hydroxide (LDH) has been widely studied as one of the most efficient OER catalysts in alkaline solution owing to the dramatically enhanced catalytic activity, which is believed to stem from the synergistic interactions between Ni and Fe species.[16, 18-21] Since the active sites for the OER process are principally located on the surface of the catalyst, the surface area could largely influence the electrocatalytic performance.[7, 22-24] Accordingly, the rational design of nanostructures for Ni-Fe LDH-based electrocatalysts by increasing the number of their exposed active sites could efficiently promote the OER activity.

Hollow nanostructures have exhibited desirable advantages as OER catalysts owing to their architectural features, such as large surface area, low density, multiple interfaces, and reduced diffusion lengths for mass transport.[25-27] Compared with single-shelled hollow structures, hollow catalysts with the multi-shelled feature exhibit apparent superiorities for electrocatalysis.[28-30] To be more specific, multi-shells provide larger surface area and better utilization of the inner space.

Moreover, the interlayers can support each other for enhanced mechanical stability. Therefore, it can be expected that the multi-shelled hollow catalysts could have improved catalytic activity per unit area with better cycling stability. Layer-by-layer strategies based on hard templates are usually employed as effective methods to construct complex hollow structures with narrow size distribution.[31, 32] However, the tedious and complex synthetic procedure is a severe issue for the practical application of complex hollow catalysts. Besides, hierarchical features of LDH based materials and different precipitation kinetics between divalent and trivalent metal cations might add extra preparation obstacles.

Herein we present a facile one-pot self-templated strategy to synthesize Ni-Fe LDH double-shelled nanocages (DSNCs) assembled by ultrathin nanosheets. Starting from spindle-like particles of MIL-88A (a metal-organic framework (MOF); MIL stands for Materials from Institut Lavoisier), double-shelled Ni-Fe LDH nanocages with hierarchical features are obtained through the simultaneous etching and coprecipitation reactions in a mixed solution. By adjusting the volume ratio between the solvent components, the shell number could be further tailored. Benefiting from the unique merits of these hierarchical hollow structures, the double-shelled Ni-Fe LDH nanocages manifest significantly enhanced electrocatalytic activity towards OER in an alkaline electrolyte.

The synthetic processes of the Ni-Fe LDH nanocages with different shells are schematically illustrated in **Figure 1**. First, uniform MIL-88A particles with smooth surface are synthesized as the sacrificial templates (Figure S1, see Supporting Information).[33] After hydrolysis reactions of urea and nickel nitrate in a mixed solution of ethanol and water, the hierarchical Ni-Fe LDH nanocages with different shells are obtained. During this formation process, MIL-88A templates can be gradually etched with the hydrolyzation reactions (Figure S2, see Supporting Information), the released Fe species coprecipitate with Ni^{2+} and OH^- ions to form thin layered Ni-Fe LDH shells. The shell number can be steadily controlled by adjusting the etching and coprecipitation rates. Specifically, more ethanol in the mixed solvent slows down the etching of MIL-88A, leading to the formation of Ni-Fe

LDH DSNCs. Whereas, more water in the mixed solvent leads to fast hydrolysis, which could only produce Ni-Fe LDH single-shelled nanocages (SSNCs) because of the fast etching of the template.

We first take the formation of Ni-Fe LDH DSNCs as an example to demonstrate the synthesis. Field-emission scanning electron microscopy (FESEM) image indicates that Ni-Fe LDH DSNCs inherit the spindle-like morphology of MIL-88A, while the smooth surface of the precursor is turned into a rough shell constructed from nanosheets (**Figure 2**a). As shown by transmission electron microscopy (TEM), the double-shelled feature of these uniform nanocages is displayed clearly by the sharp contrast between the hierarchical shells and the central void space (Figure 2b). TEM images of an individual hollow particle further reveal that the inner shell is also composed of ultrathin nanosheets (Figure 2c,d). Furthermore, the folded edges or wrinkles of these nanosheets indicate the ultrathin nature (Figure 2d). X-ray diffraction (XRD) pattern of the Ni-Fe LDH DSNCs can be assigned to a typical LDH phase, indicating the complete consumption of the MIL-88A precursor during the reaction (Figure S3, see Supporting Information). In addition, all the diffraction peaks are significantly broadened, which is likely due to the small crystallites sizes and stacking faults. Energy-dispersive X-ray (EDX) spectroscopy analysis validates the presence of Ni, Fe, and O in the Ni-Fe LDH DSNCs with a Ni/Fe atomic ratio around 0.93 (Figure S4, see Supporting Information). To investigate the spatial distribution of different elements, a line profile and elemental mapping analysis in the scanning TEM (STEM) mode are carried out on a single Ni-Fe LDH DSNC. A high-angle annular dark field-STEM image (Figure 2e) and the corresponding linear scan results (Figure 2f) imply that the distributions for different elements are quite distinct. The concentrations of Ni and O species are higher in the inner layer compared with those in the outmost shell. Whereas, the Fe species are richer in the outer shell. EDX elemental mapping images also confirm the differentiated distributions of Ni, Fe and O throughout the double-shelled nanocages (Figure 2g-i). The above results suggest the different migration directions for different elements in the synthesis.

As for Ni-Fe LDH SSNCs, the morphological examination confirms the hollow nature of these formed particles (Figure S5a,b, see Supporting Information). Compared with Ni-Fe LDH DSNCs, this Ni-Fe LDH hollow sample has a different Ni/Fe atomic ratio of 2.50, although the XRD pattern reveals the similar LDH phase (Figure S5c,d, see Supporting Information). Moreover, the smaller core of the yolk-shelled intermediate for Ni-Fe LDH SSNCs validates the faster etching of the MIL-88A template (Figure S6, see Supporting Information). To further verify our hypothesis for the synthesis, some control experiments are carried out. When ethanol is employed as the sole solvent, the kinetics of hydrolysis is very slow to etch the inner core (Figure S7a, see Supporting Information). On the contrary, pure water system could induce faster etching of MIL-88A and accelerate the growth of the LDH nanosheets (Figure S7b, see Supporting Information).

X-ray photoelectron spectroscopy (XPS) measurements are conducted to investigate the elemental compositions and the detailed surface electronic states. As shown in **Figure 3**a, the survey spectra of both Ni-Fe LDH samples reveal the coexistence of Ni, Fe, and O in the obtained samples. XPS spectra of Ni 2p for the two samples indicate two spin-orbit peaks with a binding energy difference about 17.7 eV, namely Ni $2p_{1/2}$ (873.43 eV) and Ni $2p_{3/2}$ (855.73 eV), confirming the predominance of Ni^{2+} valence form (Figure 3b).[34] The Fe species in both samples are found to be mostly in the +3 oxidation state according to the high-resolution XPS spectra of Fe 2p (Figure 3c).[21]

Next, the electrocatalytic OER activity of the Ni-Fe LDH DSNCs is evaluated in an alkaline solution (1.0 M KOH) using carbon paper as the catalyst support. The electrocatalytic properties of Ni-Fe LDH SSNCs and carbon paper are also studied as the references. **Figure 4**a shows the *iR*-compensated polarization curves of the two catalysts as well as the carbon paper support recorded by the linear sweep voltammetry (LSV) mode. It can be observed that the Ni-Fe LDH DSNC catalyst shows a remarkably higher current density than the Ni-Fe LDH SSNC sample at the same overpotential (η). A broad redox peak is observed starting at around 1.4 V relative to the reversible hydrogen electrode (RHE), which is assigned to the oxidation of Ni^{2+} to Ni^{3+}. As can be seen, the

OER activity of the carbon paper support can be neglected in this experiment. To reach a current density of 20 mA cm^{-2}, the Ni-Fe LDH DSNC catalyst requires an overpotential of only 246 mV, which is 15 mV lower than that of Ni-Fe LDH SSNCs (Figure 4b). Moreover, the OER kinetics of Ni-Fe LDH DSNCs is much faster than that of Ni-Fe LDH SSNCs. Specifically, the current density of Ni-Fe LDH DSNCs could reach 50 mA cm^{-2} at the η of 272 mV, which is 28 mV lower than that of Ni-Fe LDH SSNCs (Figure 4b). At the η of 270 mV (Figure 4c), the current density of Ni-Fe LDH DSNCs (48 mA cm^{-2}) is much higher than that of Ni-Fe LDH SSNCs (26 mA cm^{-2}). The Tafel plots of catalysts are further calculated based on the LSV curves. As shown in Figure 4d, the Ni-Fe LDH DSNC catalyst exhibits obviously better kinetics compared with Ni-Fe SSNCs as proved by the much smaller Tafel slope of the former (71 versus 117 mV dec^{-1}). The OER activity of Ni-Fe LDH DSNCs also compares favourably with those of many Ni-Fe LDH based electrocatalysts (Table S1, see Supporting Information).[19, 21, 34-40]

To investigate the possible reason for the enhanced electrocatalytic activity of Ni-Fe LDH DSNCs, the electrochemically active surface area (ECSA) is estimated by determining the double-layer capacitances (C_{dl}). Specifically, cyclic voltammograms (CVs) at different scan rates are performed in a non-Faradaic potential range (0.90-1.00 V versus RHE) to obtain the capacitive current associated with C_{dl} for the Ni-Fe LDH hollow structures with different shells (Figure S8, see Supporting Information). Then, the C_{dl} can be estimated by plotting the $\Delta j/2 = (j_a - j_c)/2$ at 0.95 V versus RHE against the scan rate (Figure 4e). The linear slope of Ni-Fe LDH DSNCs is greater than that of Ni-Fe LDH SSNCs. This suggests the larger ECSA of Ni-Fe LDH DSNCs which should be responsible for the superior electrocatalytic OER activity. The enhanced ECSA of Ni-Fe LDH DSNCs might be derived from their unique double-shelled structure and abundant ultrathin nanosheets. Besides, the electrochemical impedance spectroscopy (EIS) characterizations also show that the double-shelled Ni-Fe LDH catalyst possesses a much smaller semicircle, indicating reduced charge transfer resistance (R_{ct}) and faster charge-transfer kinetics than the single-shelled sample

(Figures S9, see Supporting Information). In addition, the increased Fe/Ni ratio in the Ni-Fe LDH DSNCs might also contribute to the enhanced electrocatalytic activity. More Fe species could prominently improve the conductivity and bring in the Ni-Fe partial-charge-transfer activation process. As a result, the intrinsic activity of the active species is improved.[41] We further evaluate the Ni-Fe LDH DSNC catalyst by a chronoamperometric measurement under a constant η of 251 mV in a 1.0 M KOH solution. The *j* value generally remains stable over 50 h with a small degradation and some fluctuation, validating the good stability of the Ni-Fe LDH DSNCs under alkaline condition (Figure 4f).

In summary, we have developed a facile one-pot strategy to controllably synthesize double-shelled Ni-Fe layered double hydroxide (LDH) nanocages as a highly efficient electrocatalyst for the oxygen evolution reaction. By rationally regulating the volume ratio of ethanol and water, the shell number of the Ni-Fe LDH nanocages can be easily controlled. Owing to the optimized chemical composition and structural advantages, the double-shelled Ni-Fe LDH nanocages manifest enhanced electrocatalytic performances towards the oxygen evolution reaction. Specifically, the catalyst based on the double-shelled nanocages could reach a current density of 20 mA cm^{-2} at a small overpotential of 246 mV, with a small Tafel slope of 71 mV dec^{-1} and excellent stability in alkaline electrolyte.

Acknowledgements

X.W.L. acknowledges the funding support from the National Research Foundation (NRF) of Singapore via the NRF Investigatorship (NRF-NRFI2016-04) and the Ministry of Education of Singapore through Academic Research Fund (AcRF) Tier-1 Funding (M4011783, RG5/17 (S)). S.Y.G. acknowledges the funding support from the National Natural Science Foundation of China (Grant no. U1804255).

References

[1] Z. P. Cano, D. Banham, S. Y. Ye, A. Hintennach, J. Lu, M. Fowler, Z. W. Chen, *Nat. Energy* **2018**, *3*, 279.

[2] Y. Kuang, M. J. Kenney, Y. T. Meng, W. H. Hung, Y. J. Liu, J. E. Huang, R. Prasanna, P. S. Li, Y. P. Li, L. Wang, M. C. Lin, M. D. McGehee, X. M. Sun, H. J. Dai, *Proc. Natl. Acad. Sci. U. S. A.* **2019**, *116*, 6624.

[3] I. E. L. Stephens, J. Rossmeisl, I. Chorkendorff, *Science* **2016**, *354*, 1378.

[4] X. F. Lu, L. Yu, X. W. Lou, *Sci. Adv.* **2019**, *5*, eaav6009.

[5] X. Tian, X. Zhao, Y.-Q. Su, L. Wang, H. Wang, D. Dang, B. Chi, H. Liu, E. J. M. Hensen, X. W. Lou, B. Y. Xia, *Science* **2019**, *366*, 850.

[6] I. Roger, M. A. Shipman, M. D. Symes, *Nat. Rev. Chem.* **2017**, *1*, 0003.

[7] Z. W. Seh, J. Kibsgaard, C. F. Dickens, I. B. Chorkendorff, J. K. Norskov, T. F. Jaramillo, *Science* **2017**, *355*, eaad4998.

[8] N. T. Suen, S. F. Hung, Q. Quan, N. Zhang, Y. J. Xu, H. M. Chen, *Chem. Soc. Rev.* **2017**, *46*, 337.

[9] B. Zhang, X. L. Zheng, O. Voznyy, R. Comin, M. Bajdich, M. Garcia-Melchor, L. L. Han, J. X. Xu, M. Liu, L. R. Zheng, F. P. G. de Arquer, C. T. Dinh, F. J. Fan, M. J. Yuan, E. Yassitepe, N. Chen, T. Regier, P. F. Liu, Y. H. Li, P. De Luna, A. Janmohamed, H. L. L. Xin, H. G. Yang, A. Vojvodic, E. H. Sargent, *Science* **2016**, *352*, 333.

[10] B. R. Wygant, K. Kawashima, C. B. Mullins, *ACS Energy Lett.* **2018**, *3*, 2956.

[11] K. Liu, C. Zhang, Y. Sun, G. Zhang, X. Shen, F. Zou, H. Zhang, Z. Wu, E. C. Wegener, C. J. Taubert, J. T. Miller, Z. Peng, Y. Zhu, *ACS Nano* **2018**, *12*, 158.

[12] D. A. Kuznetsov, B. H. Han, Y. Yu, R. Rao, J. Hwang, Y. Román-Leshkov, Y. Shao-Horn, *Joule* **2018**, *2*, 225.

[13] Y. Wang, B. Kong, D. Zhao, H. Wang, C. Selomulya, *Nano Today* **2017**, *15*, 26.

[14] D. Wang, D. Astruc, *Chem. Soc. Rev.* **2017**, *46*, 816.

[15] G. Zhang, G. Wang, Y. Liu, H. Liu, J. Qu, J. Li, *J. Am. Chem. Soc.* **2016**, *138*, 14686.

[16] L. Yu, J. F. Yang, B. Y. Guan, Y. Lu, X. W. Lou, *Angew. Chem., Int. Ed.* **2018**, *57*, 172.

[17] J. W. Nai, B. Y. Guan, L. Yu, X. W. Lou, *Sci. Adv.* **2017**, *3*, e1700732.

[18] M. Gong, H. Dai, *Nano Res.* **2015**, *8*, 23.

[19] L. N. Dang, H. F. Liang, J. Q. Zhuo, B. K. Lamb, H. Y. Sheng, Y. Yang, S. Jin, *Chem. Mater.* **2018**, *30*, 4321.

[20] R. Chen, S. F. Hung, D. J. Zhou, J. J. Gao, C. J. Yang, H. B. Tao, H. B. Yang, L. P. Zhang, L. L. Zhang, Q. H. Xiong, H. M. Chen, B. Liu, *Adv. Mater.* **2019**, 1903909.

[21] Q. Wang, L. Shang, R. Shi, X. Zhang, Y. F. Zhao, G. I. N. Waterhouse, L. Z. Wu, C. H. Tung, T. R. Zhang, *Adv. Energy Mater.* **2017**, *7*, 1700467.

[22] Y. P. Zhu, C. X. Guo, Y. Zheng, S. Z. Qiao, *Acc. Chem. Res.* **2017**, *50*, 915.

[23] C. X. Guo, Y. Zheng, J. R. Ran, F. X. Xie, M. Jaroniec, S. Z. Qiao, *Angew. Chem., Int. Ed.* **2017**, *56*, 8539.

[24] Y. Jiao, Y. Zheng, M. Jaroniec, S. Z. Qiao, *Chem. Soc. Rev.* **2015**, *44*, 2060.

[25] K. Huang, Y. Sun, Y. Zhang, X. Wang, W. Zhang, S. Feng, *Adv. Mater.* **2019**, *31*, e1801430.

[26] G. Prieto, H. Tueysuez, N. Duyckaerts, J. Knossalla, G.-H. Wang, F. Schueth, *Chem. Rev.* **2016**, *116*, 14056.

[27] L. Zhou, M. F. Shao, M. Wei, X. Duan, *J. Energy Chem.* **2017**, *26*, 1094.

[28] L. Yu, H. Hu, H. B. Wu, X. W. Lou, *Adv. Mater.* **2017**, *29*, 1604563.

[29] W. Zhu, Z. Chen, Y. Pan, R. Dai, Y. Wu, Z. Zhuang, D. Wang, Q. Peng, C. Chen, Y. Li, *Adv. Mater.* **2018**, *30*, e1800426.

[30] G. Zhan, P. Li, H. C. Zeng, *Adv. Mater.* **2018**, *30*, e1802094.

[31] Z. Y. Wang, Z. C. Wang, H. B. Wu, X. W. Lou, *Sci. Rep.* **2013**, *3*, 1391.

[32] X. J. Wang, J. Feng, Y. C. Bai, Q. Zhang, Y. D. Yin, *Chem. Rev.* **2016**, *116*, 10983.

[33] J. T. Zhang, Z. Li, Y. Chen, S. Y. Gao, X. W. Lou, *Angew. Chem., Int. Ed.* **2018**, *57*, 10944.

[34] D. J. Zhou, S. Y. Wang, Y. Jia, X. Y. Xiong, H. B. Yang, S. Liu, J. L. Tang, J. M. Zhang, D. Liu, L. R. Zheng, Y. Kuang, X. M. Sun, B. Liu, *Angew. Chem., Int. Ed.* **2019**, *58*, 736.

[35] T. Y. Wang, G. Nam, Y. Jin, X. Y. Wang, P. J. Ren, M. G. Kim, J. S. Liang, X. D. Wen, H. Jang, J. T. Han, Y. H. Huang, Q. Li, J. Cho, *Adv. Mater.* **2018**, *30*, 1800757.

[36] C. Andronescu, S. Barwe, E. Ventosa, J. Masa, E. Vasile, B. Konkena, S. Moller, W. Schuhmann, *Angew. Chem., Int. Ed.* **2017**, *56*, 11258.

[37] Y. Jia, L. Z. Zhang, G. P. Gao, H. Chen, B. Wang, J. Z. Zhou, M. T. Soo, M. Hong, X. C. Yan, G. R. Qian, J. Zou, A. J. Du, X. D. Yao, *Adv. Mater.* **2017**, *29*, 1700017.

[38] Z. Cai, D. J. Zhou, M. Y. Wang, S. M. Bak, Y. S. Wu, Z. S. Wu, Y. Tian, X. Y. Xiong, Y. P. Li, W. Liu, S. Siahrostami, Y. Kuang, X. Q. Yang, H. H. Duan, Z. X. Feng, H. L. Wang, X. M. Sun, *Angew. Chem., Int. Ed.* **2018**, *57*, 9392.

[39] G. B. Chen, T. Wang, J. Zhang, P. Liu, H. J. Sun, X. D. Zhuang, M. W. Chen, X. L. Feng, *Adv. Mater.* **2018**, *30*, 1706279.

[40] Z. Yuan, S.-M. Bak, P. Li, Y. Jia, L. Zheng, Y. Zhou, L. Bai, E. Hu, X.-Q. Yang, Z. Cai, Y. Sun, X. Sun, *ACS Energy Lett.* **2019**, *4*, 1412.

[41] L. Trotochaud, S. L. Young, J. K. Ranney, S. W. Boettcher, *J. Am. Chem. Soc.* **2014**, *136*, 6744.

Figures and Captions

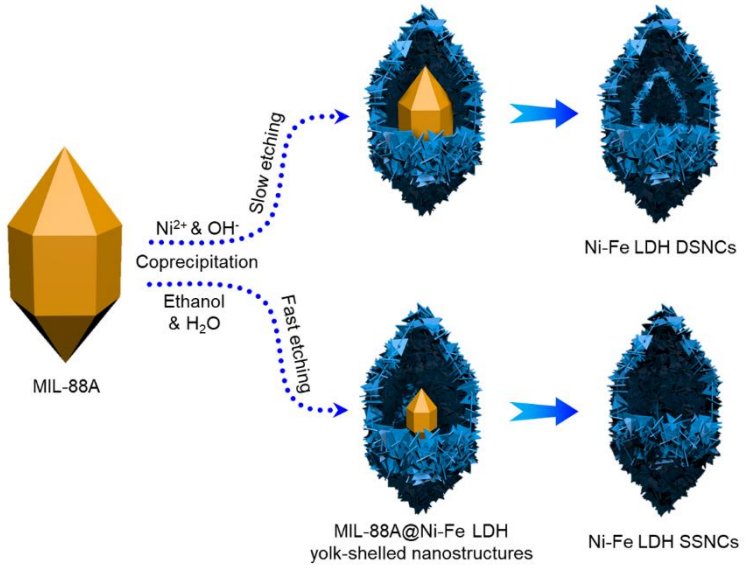

Figure 1. Schematic illustration of the formation of Ni-Fe LDH nanocages with tunable shells via a self-templated strategy.

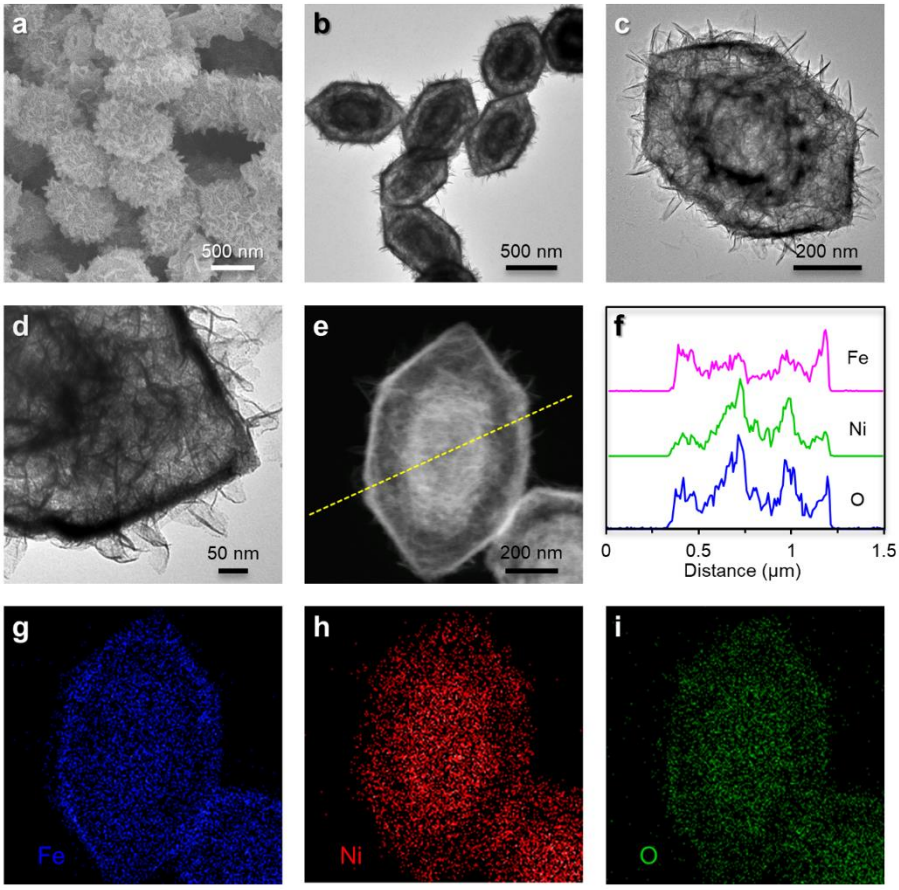

Figure 2. (a) FESEM and (b-d) TEM images of Ni-Fe LDH DSNCs. (e) HAADF-STEM image, (f) the corresponding linear distributions, and (g-i) mapping results of different elements for an individual Ni-Fe LDH DSNC.

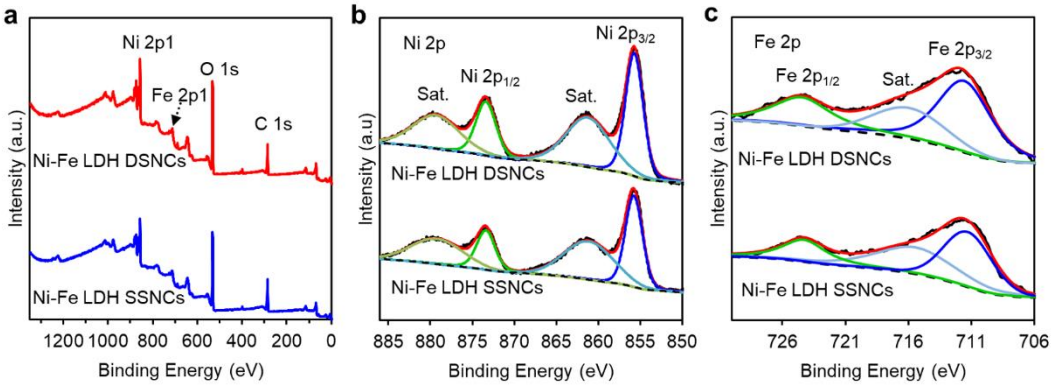

Figure 3. XPS spectra of (a) survey, (b) Ni 2p, and (c) Fe 2p for Ni-Fe LDH nanocages with different shells.

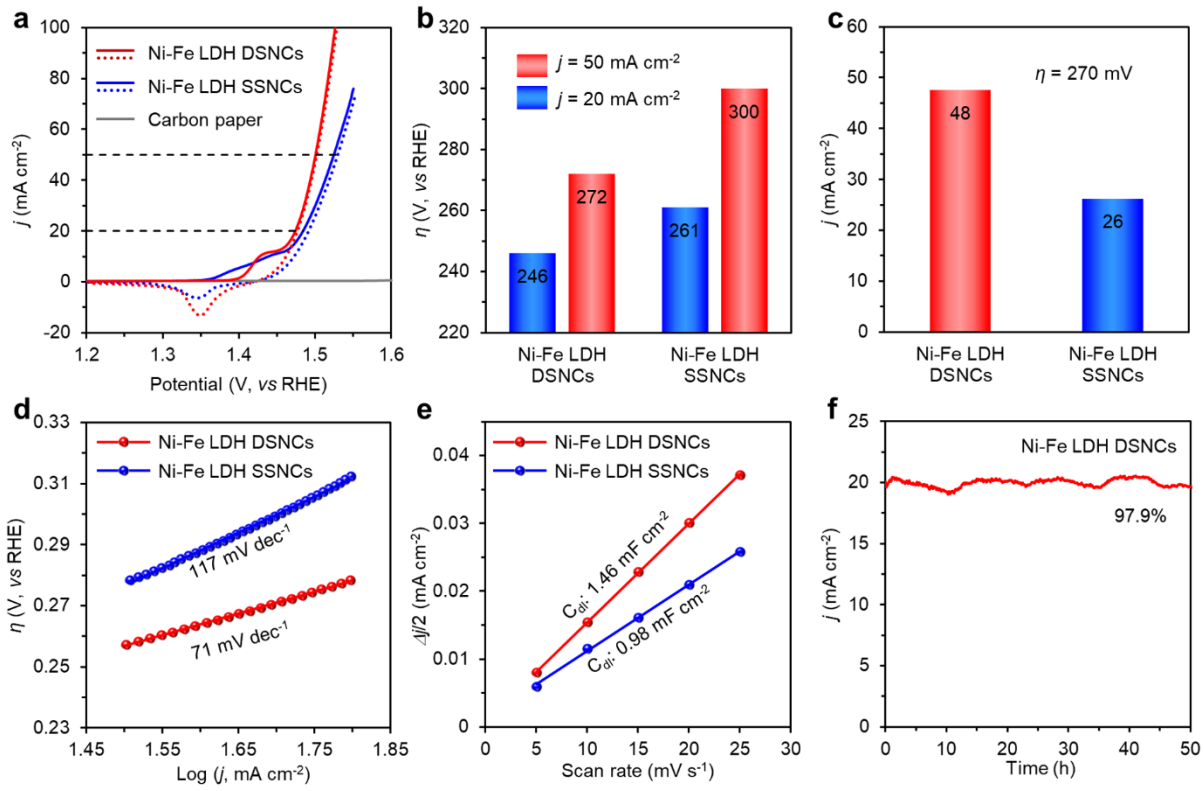

Figure 4. (a) LSV curves of Ni-Fe LDH catalysts and carbon paper. (b) η for different current densities, (c) current density at η = 270 mV, (d) Tafel slopes, and (e) capacitive $\Delta j/2 = (j_a - j_c)/2$ as a function of the scan rate for Ni-Fe LDH catalysts with different shells. j_a represents the anodic current density, j_c represents the cathodic current density. (f) Time dependence of current density of the Ni-Fe LDH DSNC catalyst at a constant η of 251 mV.

For Table of Content Entry

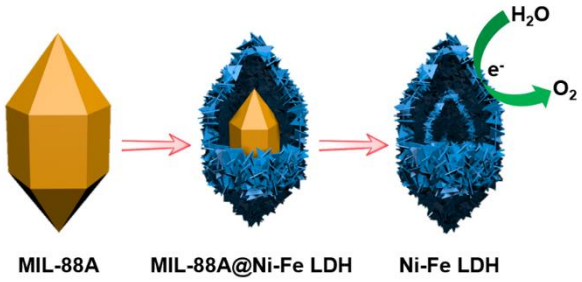

Hierarchical Ni-Fe layered double hydroxide (LDH) nanocages with different shells have been designed and synthesized via a one-pot self-templated method. Benefiting from the optimized architecture and improved reaction kinetics, the Ni-Fe LDH nanocages demonstrate appealing electrocatalytic activity for the oxygen evolution reaction in an alkaline medium. Particularly, the double-shelled nanocages require an overpotential of 246 mV to reach a current density of 20 mA cm^{-2} and are stable over 50 h.